CHANDRA AND XMM-NEWTON SPECTROSCOPY OF NGC 5548

K. C. Steenbrugge[a], J. S. Kaastra [a] R. Edelson [b]

[a]SRON National Institute for Space Research, Sorbonnelaan 2, 3584 CA Utrecht, The Netherlands

[b]Department of Physics and Astronomy, University of California, Los Angeles; Los Angeles, CA 90095-1562, USA

We present results on the 140 ks RGS and the 350 ks LETGS observation of NGC 5548. The warm absorber found from these X-ray observations spans three orders of magnitude in ionization parameter, from O III, which is as lowly ionized as the warm absorber detected in the UV band, to Fe XXIV. For O VI the column density determined from our X-ray data is an order of magnitude larger than the column density measured in previous UV observations. We conclude that there is substantially more low ionized material than previously deduced from UV observations. However, only a few percent of the warm absorber detected in the X-rays is lowly ionized.

1. Introduction

The immediate environment of active galactic nuclei (AGN) is poorly understood. The black hole is fed from an accretion disk, which becomes visible through high energy radiation. Possibly powered by radiation pressure, an outflowing wind is formed from the accretion disk. In some AGN, the wind is visible through its continuum and line absorption of the radiation from the nucleus. These absorption lines were already detected in the UV part of the spectrum [1], and have now been confirmed in the X-ray spectra [2].

NGC 5548, a Seyfert 1 galaxy, has been well studied in X-rays due to its relative X-ray brightness, and the fact that it is a nearby active galactic nucleus with a redshift of z=0.01676 [3]. This Seyfert galaxy was studied in detail with *ROSAT* [4], which detected an O VII and O VIII K-shell edge, and concluded that there was a warm absorber present. Therefore, NGC 5548 is an ideal Seyfert 1 galaxy to study with the high resolution spectroscopy instruments onboard of *XMM-Newton* and *Chandra* .

2. Observation

Table 1 lists the observations of NGC 5548 taken with the high resolution instruments onboard *Chandra* and XMM-*Newton*. Of the five high resolution X-ray observations, only the two last observations have a high S/N ratio, due to the longer exposure times. Therefore, we only discuss the last two observations. For *XMM-Newton* the Reflection Grating Spectrometer (RGS) was in the standard mode. The Low Energy Transmission Grating (LETG) was used in combination with the High Resolution Camera, so as to also obtain spectral data above 40 Å. The *XMM-Newton* data were reduced using the developer's version of the *XMM-Newton* data analysis package SAS version 5.3, which comprises a correct calibration of the effective area and the instrumental O-edge. The latter is important as the 1s-2p absorption lines of O II and O III are cosmologically redshifted toward the instrumental O I edge. The fluxed spectrum of both RGS is depicted in Fig. 1. For the *Chandra* data the data reduction is described by Kaastra et al. [7]. In general the procedure followed has a wavelength accuracy between 2 and 15 mÅ, while the effective area is accurate to about 10% for the wavength range discussed here. All the spectral analysis was done with the SPEX package [9].

3. Spectral Variability

We tested all datasets on possible variations in the warm absorber over the $\sim$ 2 year time span, but were limited by the rather large error bars for the first observations. In practice we thus compared the last two results, with a seperation of six months. Although the flux was $\sim$ 50 % lower during the LETGS observation, no spectral changes were detected with respect to the long RGS observation. All column densities determined were consistent within 3 σ and mostly within 1 σ. During both observations the flux changed, but due to the already large error bars, no spectral variability was detected within one observation. As

Table 1
High resolution X-ray observations of NGC 5548. LETG is here in combination with the HRC, HETG in combination with ACIS.

Date	Instruments	Exposure (s)	References
1999 December 11	*Chandra* :LETG	86400	[2,7]
2000 February 5	*Chandra* :HETG	83000	[8,7]
2000 December 24	*XMM-Newton* : RGS	28000	noisy spectrum, low count rate
2001 July 09 till 12	*XMM-Newton* : RGS	137000	[5]
2002 January 16 till 18	*Chandra* : HETG	153900	[6]
2002 January 18 till 21	*Chandra* : LETG	350000	[6]

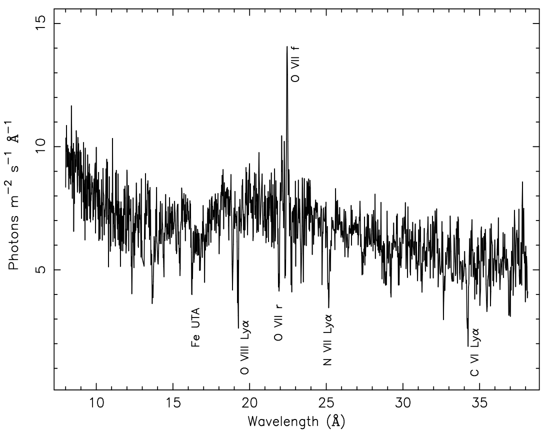

Figure 1. The fluxed spectrum of NGC 5548, RGS 1 and 2 are added together and no error bars are plotted for clarity. The typical 1 σ error on the data is 1 photon m^{-2} s^{-1} Å^{-1}. Some of the strongest features are identified.

we see the higher order lines of both O VIII and C VI Ly series as well as some inner-shell lines, which have an optical depth near unity, we can exclude a systematic variability of the warm absorber within a timespan of 6 months to a precision of 50%. The lack of spectral variability, although the continuum did vary significantly, is important in constraining the location of the X-ray warm absorber.

For the forbidden line of O VII, which is detected in emission, we find no variability, see Table 2. This is consistent with the conclusion that the O VII forbidden line is formed at a distance of 1 pc from the central source [15]. This line seems thus to be formed in the narrow-line region, and

Table 2
Comparison of the O VII forbidden line from four different observations, excluding the first and noisy RGS spectrum.

Instr.	year	v^a	σ_v^a	flux^b
LETGS	1999	0 ± 50	<330	0.8 ± 0.3
HETGS	2000	-70 ± 100	<310	0.8 ± 0.2
RGS	2001	-110 ± 80	<490	0.9 ± 0.1
LETGS	2002	-150 ± 100	<330	0.8 ± 0.1

^{a} km s^{-1}
^{b} ph m^{-2} s^{-1}

also has, in contrast to the detected absorption lines, no detected outflow velocity. This all seems to indicate that the O VII forbidden line is probably not part of the X-ray warm absorber.

4. Detailed Analysis

4.1. Absorption and emission by oxygen

A detail from the wavelength region with the O VII forbidden line as well as the O VI absorption line is shown in Fig. 2. Note that the inter-combination line (at 21.804 Å rest wavelength) is missing. Actually, in none of the three data sets it is detected by more than 1 σ significance. In Fig. 2 we see some excess emission at 21.744 Å. This is shifted by 0.06 Å from the expected position of the inter-combination line. The relative wavelength accuracy of RGS is 2 mÅ. Assuming that the inter-combination and forbidden lines are formed at the same distance from the ionizing source and under the same conditions, a blueshift of 620 km s^{-1} is inconsistent with the lack of blueshift for the forbidden line. However, as the forbidden line is strong, models predict that even tenuous gasses should produce a weak but detectable inter-combination line. One possi-

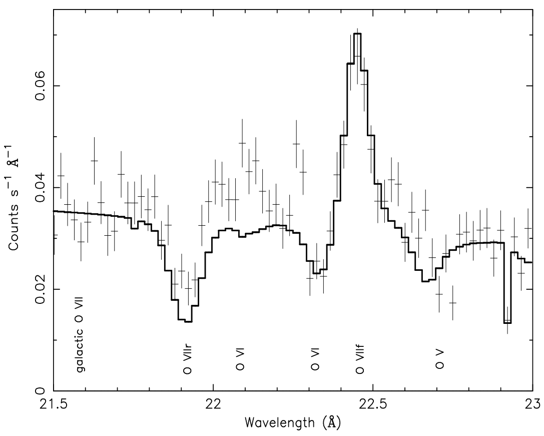

Figure 2. Detail of the RGS 1 spectrum showing the O VII triplet as well as absorption lines for O VI and O V. The galactic O VII absorption line is also indicated.

ble explanation is that the inter-combination line blends with an O VI absorption line at 21.79 Å.

Another emission feature for oxygen is the radiative recombination continuum (RRC) of O VII between 16.9 and 17 Å (see Fig. 3). As there is severe blending with iron absorption lines, we approximated the RRC simply with a delta function. We find a 2 σ detection for this RRC and the narrowness of the feature (unresolved by the instrument) indicates a low temperature. The flux is 0.06 ± 0.03 ph m^{-2} s^{-1} which is consistent with the 0.06 ± 0.10 ph m^{-2} s^{-1} value as determined from the LETGS spectrum [7].

For O VIII Lyα we detect the higher order lines up to Lyδ, with even hints of Lyϵ. These higher order lines are important in variability studies as they have an optical thickness of order unity. These higher order lines as well as the highly ionized iron lines that are detected in this wavelength range are shown in Fig. 4.

4.2. Absorption by iron

Iron is the best indicator for the ionization structure of the warm absorber, as it has absorption lines in the RGS band from neutral Fe I to the highly ionized Fe XXIV and in the LETGS band to Fe XXVI. For NGC 5548 we detect absorption from Fe VI to Fe XXIV. The lowest ionization component is represented by the UTA [13] formed from inner-shell transitions of Fe VI through Fe XI. These ions represent the lower ionized iron ions. Fig. 3 gives a detailed view of the spectrum between 16 and 17.5 Å, where the UTA is located. Note that although there are some individual absorption features visible, the dominant effect of the UTA is the depression of the continuum due to an unresolved blend of transitions with small cross-sections. The UTA clearly shows the importance of these inner-shell transitions in determining the continuum correctly.

The moderately ionized component is represented by Fe XIII through Fe XIX, where we only find an upper limit for Fe XII and Fe XIV. The highest ionized component is represented by absorption by Fe XIX through Fe XXIV. For Fe XIX through Fe XXII we detect a multitude of absorption lines. For Fe XXIII and Fe XXIV only two absorption lines are detected, resulting in rather uncertain velocity determinations.

5. Discussion

5.1. Connecting the X-ray and UV warm absorber

For all ions detected in absorption we find an outflow velocity, which averages to -350 ± 250 km s^{-1}, and none can be resolved with current X-ray instrumentation. However, no relation between outflow velocity and ionization was detected, possibly due to the large error bars on the velocity measurements. All the ions detected in X-rays have a similar outflow velocity to those detected in the UV band. This seems to indicate that there is a physical correlation between both warm absorbers. The detection of O VI in the X-ray band, first with the RGS instrument and also in the later LETGS observation confirms that both absorbers are the same, although we detect an order of magnitude larger column density in the X-rays than previously claimed from the UV. This seems to indicate that the UV detected column densities have been systematically underestimated. For a more detailed analysis see Arav et al. [10].

5.2. Derived total column density

The derived absorbing column density per ion versus the ionization parameter is plotted in Fig. 5. In the Figure we use the ionization parameter corresponding to the state with maximum column density. In reality, however, the ion is produced over a range of ionization states. Fig. 5

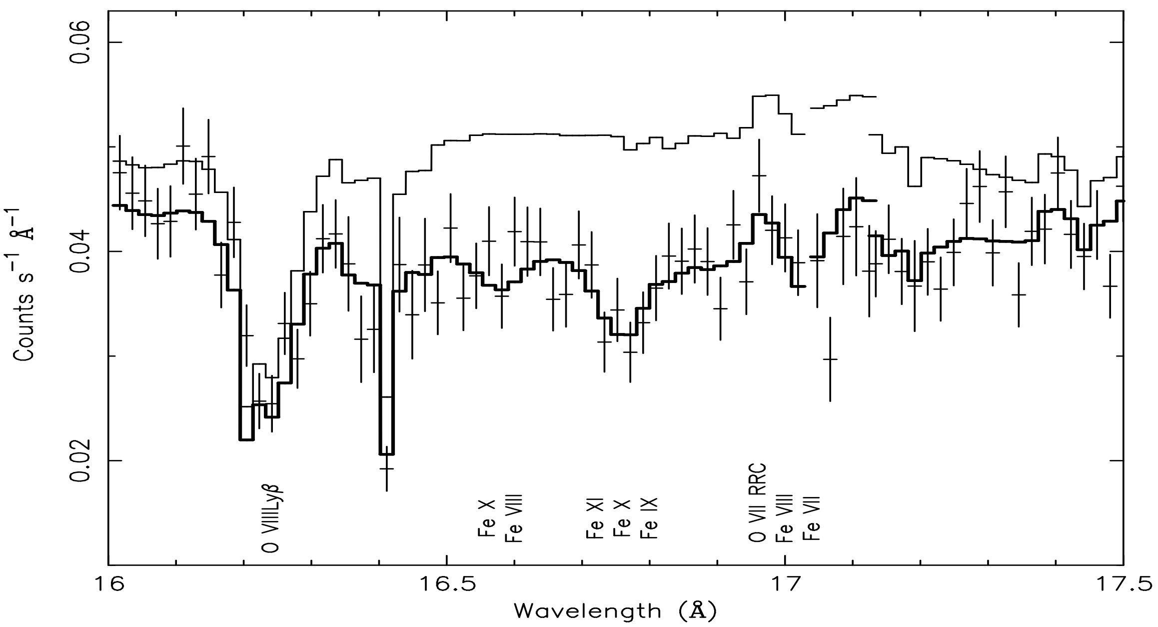

Figure 3. Detail of the first order RGS spectrum showing the UTA between 16 and 17.5 Å. The thick line is the best fit through the data, the thin line indicates the same model if we set the iron abundance of Fe VI – Fe XI to 0. A dead pixel occurs at 16.4 Å. The gaps in the model at 17.05 and 17.15 Å are due to missing data. Only the deepest features are labeled.

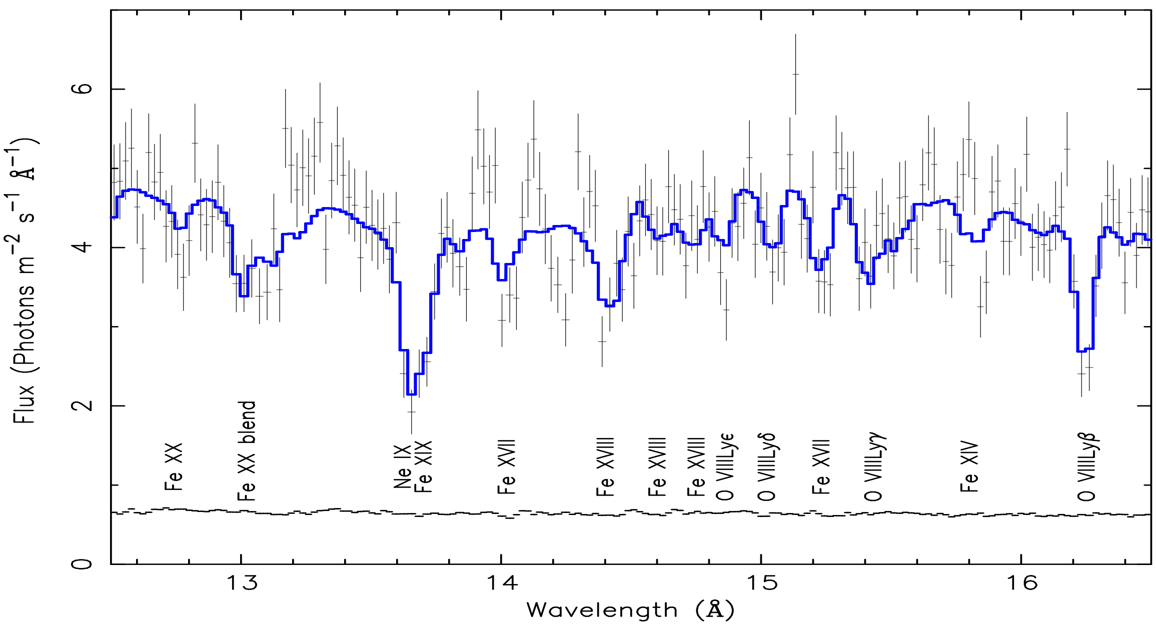

Figure 4. Detail of the LETGS spectrum between 12.5 and 16.5 Å. Note the higher order O VIII lines as well as the many iron and some Ne lines.

assumes a continuous ionization distribution, and is dependent on the spectral energy distribution (SED) in our models with XSTAR [11].

5.3. Abundances

In general the abundances found are consistent with solar, using the values of Anders & Grevesse [12]. An exception is iron, for which lowly ionized iron is overabundant compared to lowly ionized oxygen, while a reverse trend occurs for highly ionized iron and oxygen. As carbon and nitrogen are consistent with oxygen, the effect is probably due to uncertainties for the lowly ionized iron ions [5].

Possible explanations for the iron overabundance are an uncertainty in the wavelength of the M-shell iron absorption lines; or if the optical depth, $\tau \gg 1$, an uncertainty in the radiative transfer models used. Another possibility is the omission of certain processes like re-emission and Bowen fluorescence in the radiative transfer models used. Finally, the iron abundance could be non-solar, although the physical process causing such an overabundance of iron in Seyfert galaxies is unknown. Non-solar abundances have been detected in IRAS 13349+2438 [13] and NGC 1068 [14].

REFERENCES

1. Mathur, S., Elvis, M. & Wilkes, B., 1995, ApJ 452, 230
2. Kaastra, J. S., Mewe, R., Liedahl, D. A., Komossa, S., Brinkman, A. C., 2000, A&A, 354, L83
3. Crenshaw, D. M. & Kraemer, S. B., 1999, ApJ, 521, 572
4. Done, C., Pounds, K. A., Nandra, K. & Fabian, A. C., 1995, MNRAS, 275, 417
5. Steenbrugge, K.C., Kaastra, J. s. & Edelson, R., accepted for A&A
6. Steenbrugge, K.C. & Kaastra, J. S., in preparation
7. Kaastra, J. S., Steenbrugge, K. C., Raassen, A. J. J., et al., 2002a, A&A, 386, 427
8. Yaqoob, T., George, I. M., Nandra, K. et al., 2001, ApJ, 546, 759
9. Kaastra, J. S., Mewe, R. & Raassen, A. J. J., 2002b, Proceedings Symposium 'New Visions of the X-ray Universe in the XMM-Newton and Chandra Era'
10. Arav, N., Kaastra, J. S., Steenbrugge, K.C., et al. accepted for ApJ
11. Kallman, T. R. & Krolik, J. H., 1999, XSTAR photoionization code,

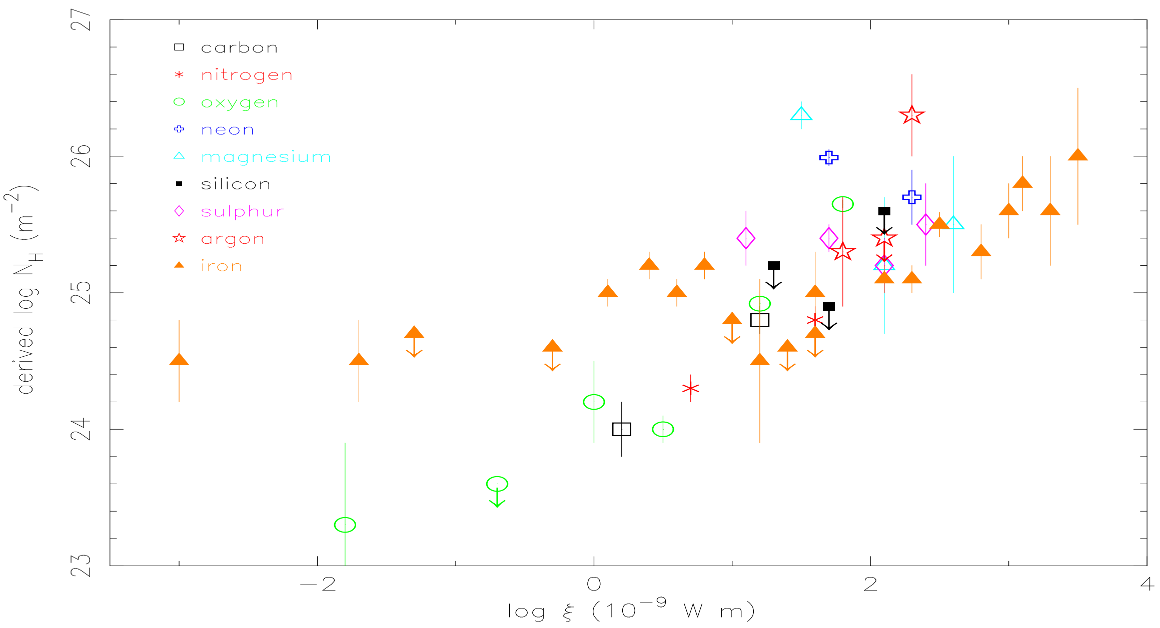

Figure 5. The derived absorbing column density per ion as derived from the measured column densities for the RGS observation. There is an increase of the derived column density with higher ionization.

ftp://legacy.gsfc.nasa.gov/software/plasma_codes/xstar/

12. Anders, E. & Grevesse, N., 1989, Geochim. Cosmochim. Acta 53, 197
13. Sako, M., Kahn, S. M., Behar, E., et al., 2001, A&A, 365, 168
14. Kinkhabwala, A., Sako, M., Behar, E., et al., 2002, ApJ, 575, 732
15. Kaastra, J. S., Steenbrugge, K. C. & Brinkman, A. C., 2003, Proceedings 'Active Galactic Nuclei: from Central Engine to Host Galaxy'

ACKNOWLEDGEMENTS

This work is based on observations obtained with *XMM-Newton* , an ESA science mission with instruments and contributions directly funded by ESA Member States and the USA (NASA). SRON National Institute for Space Research is supported financially by NWO, the Netherlands Organization for Scientific Research. RE acknowledges support from the NASA *XMM-Newton* grant NAG5-10032.